Publishing Excellence Inspiring Progress
ARISTON PUBLICATIONS
MatSci Express
ISSN: 2997-8440 www.aristonpubs.com/matsci-express https://doi.org/10.69626/mse.2024.0278

RESEARCH ARTICLE

Modelling the Optical Properties of Gold Nanoparticles using COMSOL Multiphysics: Influence of Geometry, Environment, and Temperature

Tigran A. Sargsian [1,2,*], Maksim Ya. Vinnichenko [3], David B. Hayrapetyan [1, 2]

ABSTRACT: This study explores the optical properties of gold (Au) nanoparticles (NPs) using COMSOL Multiphysics simulation software, focusing on how these properties depend on particle geometry, surrounding environment, and temperature. A comprehensive range of nanoparticle shapes—including nanospheres, nanorods, core/shell structures, nanocubes, icosahedral shapes, and nanopeanuts—were analyzed, each with varying sizes and placed in different environments such as air, water, and silica glass. Temperature effects were studied from room temperature to 1200K, allowing for an in-depth understanding of thermal influences on optical behavior. The dielectric function of the gold nanoparticles was constructed as a function of both particle size and temperature to accurately account for their impact on optical responses. The study specifically investigated absorption, scattering, and extinction cross-sections for these nanoparticles, comparing the simulation results with existing literature. A strong agreement was observed between the modeled data and previously reported findings, validating the approach. The simulations provide key insights into the size- and temperature-dependent shifts in localized surface plasmon resonance (LSPR), crucial for applications in fields such as biomedicine, thermal therapy, and imaging. These findings are particularly useful in designing gold nanoparticles with tailored optical properties for targeted applications, including drug delivery and diagnostic imaging. This work represents a holistic approach to modeling the optical properties of gold nanoparticles, addressing both geometrical and environmental influences as well as thermal effects, providing a valuable tool for future nanoparticle-based technologies.

Keywords: Gold Nanoparticles, Localized Surface Plasmon Resonance, Size-Dependent Optical Properties, Temperature Effects, COMSOL Multiphysics Simulation.

Received: 21 June 2024; Revised: 17 July 2024; Accepted: 30 July 2024; Published Online: 11 August 2024

1. INTRODUCTION

Gold (Au) has been one of the most sought-after materials by humankind for thousands of years, admired for its distinctive properties such as luster, malleability, and chemical inertness. These properties make gold highly durable, contributing to the longevity of gold artifacts and products [1-4]. However, in recent decades, with advances in nanotechnology, gold has gained a new level of significance due to the unique properties that emerge when it is reduced to the nanoscale. Gold nanoparticles (Au NPs), specifically, exhibit a wide range of novel physical, chemical, and optical behaviors, which have transformed gold nanoparticle research into an important and distinct subdiscipline within nanoscience.

The study of Au NPs focuses on understanding how their properties—particularly optical ones—change with variations in particle size, shape, and surrounding environment. One of the most notable phenomena in this

[1] Russian-Armenian University, Yerevan 0051, Armenia.
[2] Institute of Chemical Physics National Academy of Science, Republic of Armenia, Yerevan 0014, Armenia.
[3] Peter the Great St. Petersburg Polytechnic University, St. Petersburg 195251, Russia.

* Author to whom correspondence should be addressed: tigran.sargsian@rau.am (T. A. Sargsian)

regard is localized surface plasmon resonance (LSPR), where conduction electrons in Au NPs oscillate in response to incident light at specific wavelengths, leading to strong absorption and scattering [5]. This plasmonic behavior is highly sensitive to the nanoparticle's size and shape, as well as its dielectric environment, making Au NPs highly tunable for specific applications.

Au NPs have been found to convert incident light energy into heat efficiently, a property with substantial biomedical potential. This capability has been harnessed in techniques such as photothermal therapy, where the heat generated by Au NPs can be used to ablate cancerous tissues [6-9]. In addition to this therapeutic application, gold nanoparticles are valuable in diagnostic imaging. Their ability to enhance X-ray absorption has been shown to improve imaging contrast, aiding in more accurate diagnostics [10-12]. Moreover, Au NPs hold promise for use in drug delivery systems, where their biocompatibility and functionalizability allow them to serve as carriers for drugs, genes, and other therapeutic agents [13-17]. The versatility of Au NPs extends beyond medicine into fields like catalysis, electronics, and environmental science [18-20].

Given these wide-ranging applications, it is crucial to have a detailed theoretical understanding of the factors that influence the optical properties of Au NPs. While several studies have been conducted in this area, they tend to focus on a singular aspect: either the effect of the nanoparticle's geometry on optical properties [21, 22] or the role of temperature in influencing these properties [23-25]. Changes in geometry, for instance, affect the wavelength of LSPR and alter the scattering and absorption cross-sections of the particles. Meanwhile, temperature affects the dielectric function of gold, shifting the resonance frequency of Au NPs and impacting their optical efficiency. Only a small number of studies have examined both of these factors together [26, 27], leaving a gap in the literature.

This study seeks to bridge that gap by providing a more holistic understanding of how both geometry and temperature jointly affect the optical behavior of gold nanoparticles. By merging these two dimensions of investigation, we aim to develop a theoretical framework that offers insight into the size- and temperature-dependent shifts in plasmon resonance. This approach could lead to more accurate modeling and optimization of Au NP-based technologies for applications ranging from photothermal therapy to sensing and imaging.

Moreover, advancements in computational tools have made it easier to simulate and predict the behavior of such complex systems. COMSOL Multiphysics simulation software, for instance, has proven to be a powerful tool in modeling the optical properties of Au NPs [28]. COMSOL allows for precise simulations of particle geometry, dielectric environment, and temperature, thereby enabling the prediction of absorption, scattering, and extinction cross-sections for nanoparticles of different shapes and sizes. The software provides a versatile platform for conducting parametric studies that would be difficult or time-consuming to carry out experimentally.

In this work, we use COMSOL Multiphysics to model a variety of gold nanoparticle shapes—nanospheres, nanorods, nanocubes, core/shell structures, icosahedral shapes, and nanopeanuts—while systematically varying their sizes, surrounding environments (air, water, silica glass), and temperature (from room temperature to 1200K). The dielectric function of Au nanoparticles is constructed as a function of both size and temperature to account for the full range of optical responses. The primary focus of this study is on key optical properties, including plasmon resonance, absorption, scattering, and extinction cross-sections, and how they change under the influence of geometry and temperature.

2. THEORETICAL MODEL

Herein, we provide a brief overview of the theoretical model applied to this study. Under the irradiation of metallic NPs by light, the oscillating electromagnetic field forces conduction electrons to shift from their initial positions and oscillate coherently. On the other hand, the Coulomb attraction between electrons and nuclei tends to bring shifted electrons back. The arising phenomena of plasma oscillations, which are confined in a NP with a size smaller than the wavelength of light, are called LSPR. Frequency of those oscillations is highly dependent on the density of electrons, geometry of NPs and the refractive index of the environment.

The abovementioned sheds light on why LSPR shows dependence on temperature. A number of factors, such as thermal expansion of NPs, different scattering processes, the dependence on temperature of the dielectric permittivity of NPs and host medium, etc., affect LSPR to a greater or lesser degree. For example, the temperature dependence of the dielectric permittivity of host medium has small impact in the case of silica host, as discussed and shown in Ref. [23].

Talking about other factors affecting LSPR, for the linear sizes of NPs R(T) after thermal volume expansion, one can write:

$$R(T) = R_0\left(1+\beta(T)\Delta T\right)^{1/3} \tag{1}$$

where R_0 is the linear size of NP at room temperature T_0=293.15K, β(T) is the thermal expansion coefficient and ΔT is the change in temperature. In its turn, the dependence of the thermal expansion coefficient on temperature is given by:

$$\beta(T) = \frac{192\rho k_B}{r_0\phi\left(16\rho - 7k_BT\right)} \tag{2}$$

where ρ=0.4759eV, ϕ=15.83nm^{-1} and r_0=0.30242nm are parameters of Morse potential, used to describe the potential of interatomic interaction in gold [23, 29]:

$$U(r)=\rho\left(e^{-2\phi(r-r_0)}-2e^{-\phi(r-r_0)}\right) \quad (3)$$

and k_B is the Boltzmann constant.

Further theoretical investigation describing the plasmonic properties of NPs is primarily concerned with selecting an appropriate dielectric function for NPs. For sufficiently large NP sizes relative to the mean free path of electrons (which is approximately 42 nm for gold [30]), the bulk dielectric function as a local response generally produces results that are in accordance with experiments [22, 31]. This approach, however, faces difficulties while describing optical properties of small NPs with sizes comparable to the mean free path. For these purposes, in their work [22], Karimi *et al.* have proposed a phenomenological modification of the Drude dielectric model to account for quantum constrains of electron oscillations in the NPs with small sizes. They have introduced a size-dependent plasma frequency in the dielectric function for describing optical properties of small NPs, which will be brought here further.

Drude has given the dielectric function model for metals based on only intraband transition ε_D [32, 33]. It was later modified by Lorentz, who has considered the contribution from bound electrons, denoted here as interband transition (IB) ε_{ib}. Hence, Drude-Lorentz dielectric function of metal, due to both intraband and interband transitions is given by [34]:

$$\varepsilon(\omega,R,T)=\varepsilon_D(\omega,R,T)+\varepsilon_{ib}(\omega,R,T) \quad (4)$$

Temperature-dependent dielectric function due to intraband transition $\varepsilon_D(\omega,R,T)$ is given by [35]:

$$\varepsilon_D(\omega,R,T)=1-\frac{\omega_p^2(R,T)}{\omega^2+i\gamma(R,T)\omega} \quad (5)$$

where $\omega_p(R,T)$ is plasma frequency, $\gamma(R,T)$ is damping parameter [36].

The size dependency for the plasma frequency term is also taken into account. The latter mainly concerns to the intraband transitions, which is reasonable since the intraband term originates from the electron oscillations in outer levels and the surface scattering effects in small regime should mostly affect these oscillations. Based on the 1/R dependence of the plasmonic peak for small NPs given in nonlocal theory [37], a similar 1/R functionality for the size dependence is considered [22]:

$$\omega_p(R,T)=\omega_{p0}\left(a+\frac{b}{R(T)}\right)\cdot\frac{1}{\sqrt{1+\beta(T)\Delta T}} \quad (6)$$

where ω_{p0}=9.08eV is the bulk plasmon frequency and the last multiplier originates from the change in the density of the free electrons in NP due to thermal expansion [23]. The parameters a and b can be obtained from the fitting and they relate to the free electron density inside the NP and to the scattering of the electrons from the NP surface, respectively. For small NPs, Karimi *et al.* in Ref. [22] have proposed the following parameters: a=1.01 and b=0.088nm.

The damping constant $\gamma(R,T)$ is determined by electron-electron, electron-phonon, and electron-defect processes, where the last term usually includes the scattering on grain boundaries, impurities, dislocations, and so on [38]. In the absence of scattering, this parameter is equal to zero. Due to negligible contribution from damping due to electron−electron scattering as it is mostly frequency dependent, the major contribution of damping is from electron−phonon scattering and electron−surface scattering [25]. For the latter two one can write:

$$\gamma_{e-ph}(T)=\gamma_0\frac{T^5\int_0^{\theta/T}\frac{z^4dz}{e^z-1}}{T_0^5\int_0^{\theta/T_0}\frac{z^4dz}{e^z-1}} \quad (7)$$

$$\gamma_{e-s}(R,T)=A\frac{v_F}{R(T)} \quad (8)$$

$$\gamma(R,T)=\gamma_{e-ph}(T)+\gamma_{e-s}(R,T) \quad (9)$$

where γ_0=0.072eV is the damping constant at room temperature, θ=165.15K is Debye temperature for gold, A=0.6 is surface scattering parameter and $v_F=1.29\cdot10^6$m/s is the Fermi velocity for gold.

As interband transition energy is very high compared to vibrational energy, it has minimal or no effect on plasmon absorption with temperature $\varepsilon_{ib}(\omega,R,T)=\varepsilon_{ib}(\omega,R)$ [39]. Also, size dependency of interband term can be neglected as the interband transitions take place from the inner states of the NP [22, 30, 34, 40]. Thus, dielectric function due to interband transition $\varepsilon_{ib}(\omega)$ is considered temperature and size-independent and is given by [23]:

$$\varepsilon_{ib}(\omega)=\varepsilon_{bulk}(\omega)-\left(1-\frac{\omega_{p0}^2}{\omega^2+i\gamma_0\omega}\right) \quad (10)$$

where value of $\varepsilon_{bulk}(\omega)$ for gold is taken from the work done by Johnson and Christy [41].

Finally, the total dielectric function can be written as:

$$\varepsilon(\omega,R,T)=\varepsilon_{bulk}(\omega)+\frac{\omega_{p0}^2}{\omega^2+i\gamma_0\omega}-\frac{\omega_p^2(R,T)}{\omega^2+i\gamma(R,T)\omega} \quad (11)$$

while for the LSPR frequency in the case of $\mathrm{Im}[\varepsilon]<<\left|\mathrm{Re}[\varepsilon]+2\varepsilon_m\right|$ one can write [23, 25]:

$$\omega_{LSPR} = \sqrt{\frac{\omega_p^2(R,T)}{1+2\varepsilon_m+\varepsilon_{ib1}} - \gamma^2(R,T)} \quad (12)$$

Here $\varepsilon_{ib1}=\mathrm{Re}[\varepsilon_{ib}]$ is the real part of interband dielectric function, which is slightly dependent on NP size and incident light frequency in the considered region, ε_m is the dielectric permittivity of host medium.

2. SIMULATION MODEL

Herein, we will describe the modeling procedure of Au NPs with the help of COMSOL Multiphysics simulation software for the further analysis of their optical properties. In electromagnetic wave scattering problems, the total wave decomposes into the incident and scattered wave components. Important physical quantities can be obtained from the scattered fields. One of the important properties is the cross section, which can be defined as the net rate at which electromagnetic energy crosses the surface of an imaginary sphere centered at the particle, divided by the incident irradiation (P_{inc}). To quantify the rate of the electromagnetic energy absorbed (W_{abs}) and scattered (W_{sca}) by the particle, the absorption (σ_{abs}) and scattering (σ_{sca}) cross sections are defined as [42]:

$$\sigma_{abs} = \frac{W_{abs}}{P_{inc}} \quad (13)$$

$$\sigma_{sca} = \frac{W_{sca}}{P_{inc}} \quad (14)$$

The extinction cross-section σ_{ext}, in turn, is simply the sum of the absorption and scattering cross sections. The total absorbed energy is derived by integrating the energy loss over the volume of the particle. The scattered energy is derived by integrating the Poynting vector over an imaginary sphere around the particle.

As it was stated, the environment and models of Au NPs have been constructed in the COMSOL Multiphysics simulation software. In the current work spherical, nanoshell, nanorod, cubical, icosahedral and nanopeanut geometries have been considered in either air, water or silica environment. The Electromagnetic Waves, Frequency Domain (marked in the program as *emw*) interface of Radio Frequency (marked in the program as RF) [43] physics was chosen for the modeling of Au NPs and calculations of their optical properties.

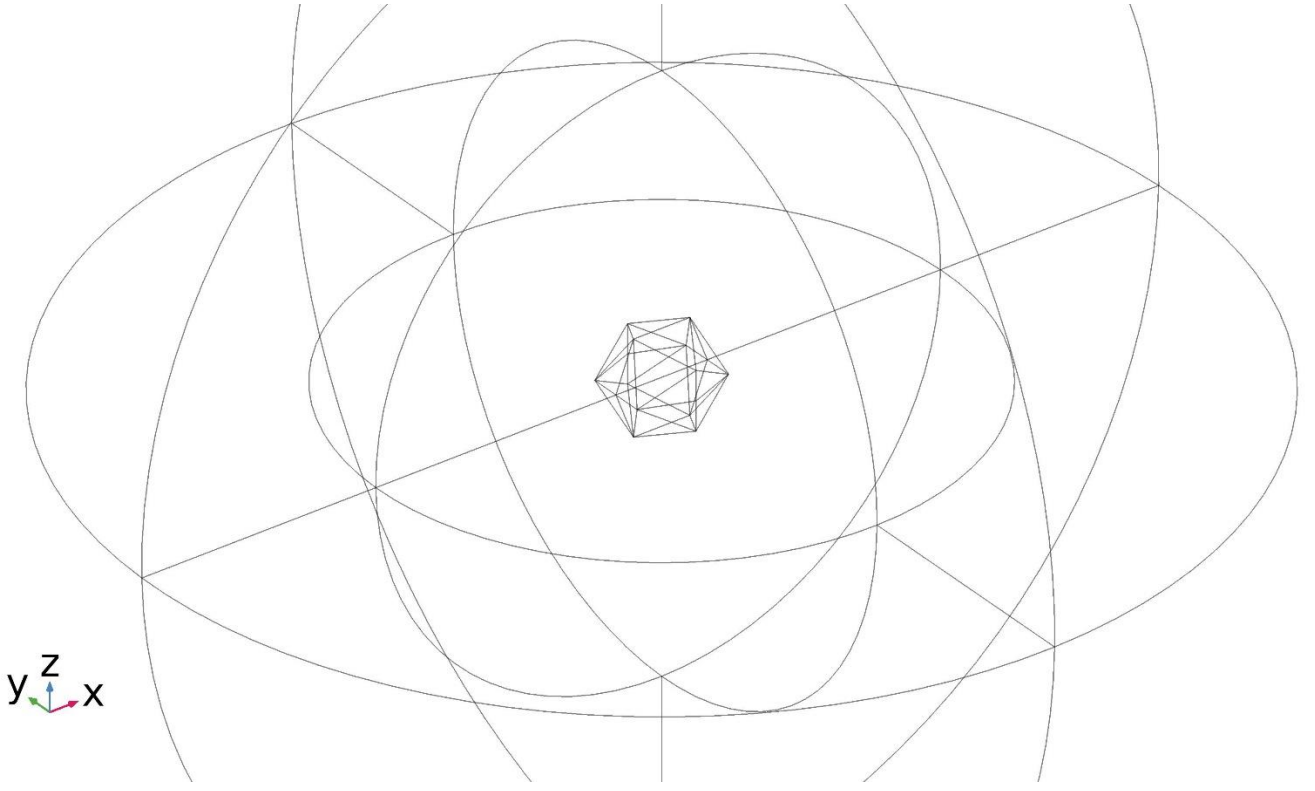

Fig. 1. The modeled geometry for the icosahedron-shaped NPs with 100 nm side length.

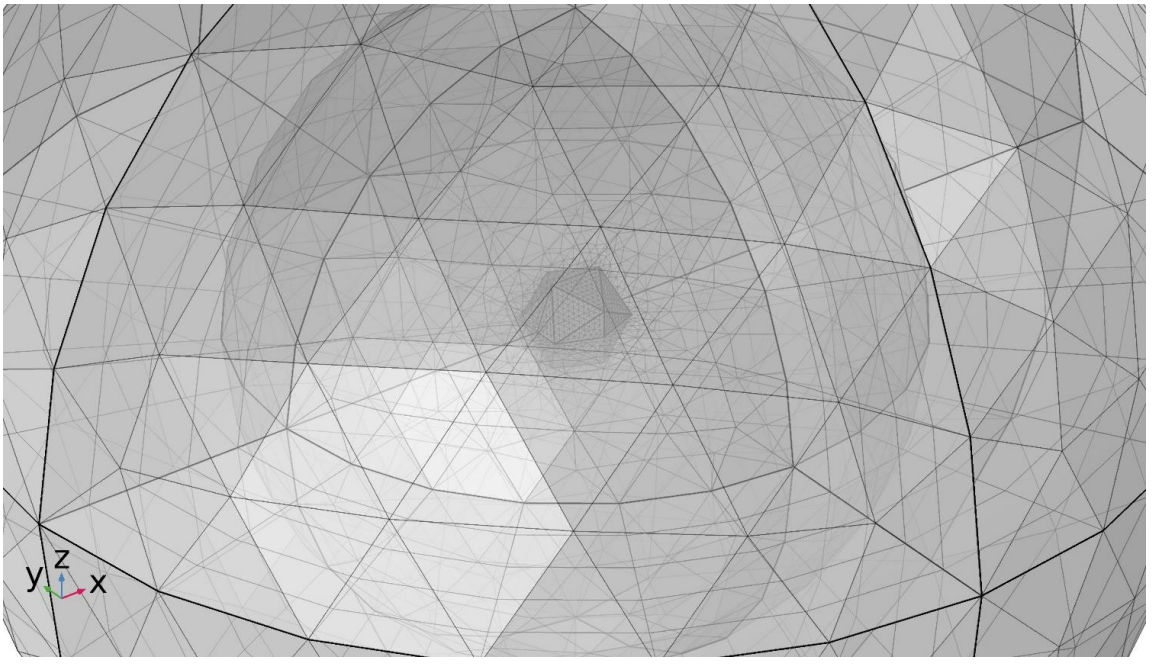

Fig. 2. The generated mesh for the icosahedron-shaped NPs with 100 nm side length.

Figure 1 presents the modeled geometry of an icosahedron-shaped nanoparticle (NP) with a side length of 100 nm. The geometry consists of three main components: the gold nanoparticle (Au NP) at the center, a 500 nm thick layer of surrounding material, and an additional 500 nm thick Perfectly Matched Layer (PML) which functions as an absorber for all outgoing wave energy. The purpose of the PML is to ensure that reflections or scattering at the boundaries do not interfere with the simulation, allowing for accurate analysis of the optical properties of the nanoparticle.

The electric field in the simulation is polarized along the z-axis, following the expression $E_z=E_0 \cdot \exp(-ik_0 n_m x)$, where k_0 is the wave number in free space and n_m represents the refractive index of the host medium. This polarized electric field interacts with the icosahedral nanoparticle, enabling the study of how the NP affects the behavior of the field.

Figure 2 illustrates the mesh generated for the icosahedron-shaped NP. A Free Tetrahedral mesh is employed within the region of interest, offering a flexible and adaptive approach to solving the electromagnetic field distribution. The mesh elements have a maximum size of 1/10th of the particle size and a minimum size of 1/40th. This ensures that the mesh resolution is fine enough to capture important physical details while maintaining computational efficiency.

The material properties of gold were sourced from the COMSOL Multiphysics Material Library, which provides extensive data for various materials based on their mechanical, optical, thermal, and electrical characteristics. The material properties are described as a function of some variable, for example, temperature or frequency. Further, one can also add his own entries for given material based on new data [44]. As presented in Figure 3, the optical properties of gold were derived from experimental data and simulations, with four key references used to represent bulk gold: Johnson and Christy (1972) [41], Rakic et al. (1998) [45], Olmon et al. (2012) [46], and Babar and Weaver (2015) [47]. Despite slight variations in the results, the qualitative differences were insignificant, making the Johnson and Christy parameters the preferred choice for the simulations, as they are widely accepted and frequently cited in the literature.

4. RESULTS AND DISCUSSION

Let us now start the discussion of the obtained results.

First, let us bring the behavior of the dielectric functions from temperature. Figure 4 presents the real part of dielectric permittivity as function from incident light energy for two sizes of NPs: 11nm (a, c) and 80nm (b, d) and at two different temperatures: room temperature (a, b) and 1200K (c, d). One can see that real parts of dielectric functions are close to the ones from Johnson and Christy's work when the NP size is comparable or larger than the mean free path of electrons and at close to room temperatures. This is quiet expected, as with the increase in NP sizes one gets closer to the bulk limit considered in the abovementioned work. When heating NPs, the difference between dielectric functions start to increase, especially for small NPs. In Figure 4a, experimental data from Ref. [48] is also presented and one can see that obtained results are very close to the latter.

Further, Figure 5 presents the dependencies for the

imaginary part of dielectric permittivity for the same sizes and at same temperatures as in Figure 4. Again, dielectric functions are close to the ones from Johnson and Christy's work when the NP size is comparable or larger than the mean free path of electrons and at close to room temperatures. However, imaginary parts differ from bulk ones especially at long wavelength range, which is due to the size-sensitive intraband contributions. Despite the overall similar behavior, there is also some quantitative mismatch between experimental results from Ref. [48] and obtained results.

Thermal expansion of a gold NP from room temperature to 1200 K was also examined. Figure 6 presents the thermal expansion of a gold NP in the range of temperatures from room to 1200K. One can see that increase in approximately 900K leads to 3.14% expansion in the linear sizes of NPs. Recall that the thermal expansion coefficient for silica glass is more than an order lower than that of gold in the discussed range of temperatures and therefore the temperature effect on the host media will be neglected.

Figure 7 presents the absorption cross-sections for a gold nanosphere with 40nm diameter in either air, water or silica glass host media. One can see that with an increase in refractive index of host media the absorption peak red-shifts in accordance with Eq. (12). Besides, the increase of n_m leads to the enlargement of the absorption cross-sections [26]. The shifts in the LSPR peak positions of gold NPs depending on the surrounding medium makes them simple and effective tools for environmental sensing.

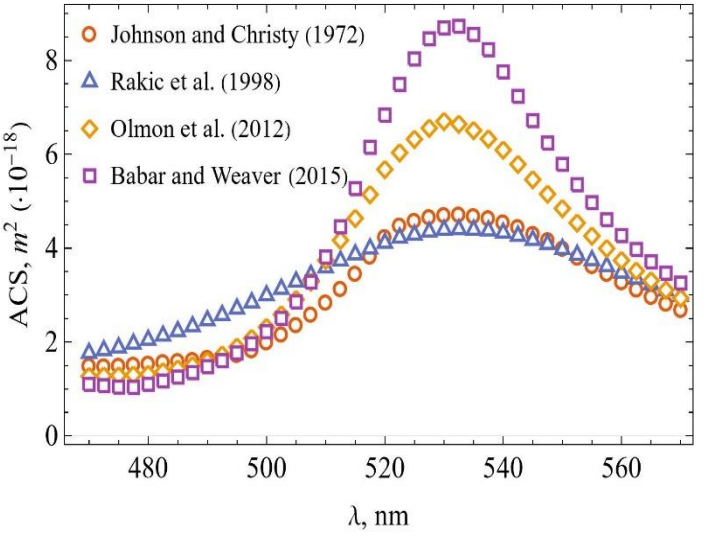

Fig. 3. Comparison of the absorption cross-section for material parameters from Johnson and Christy (1972) [41], Rakic *et al.* (1998) [45], Olmon *et al.* (2012) [46], Babar and Weaver (2015) [47].

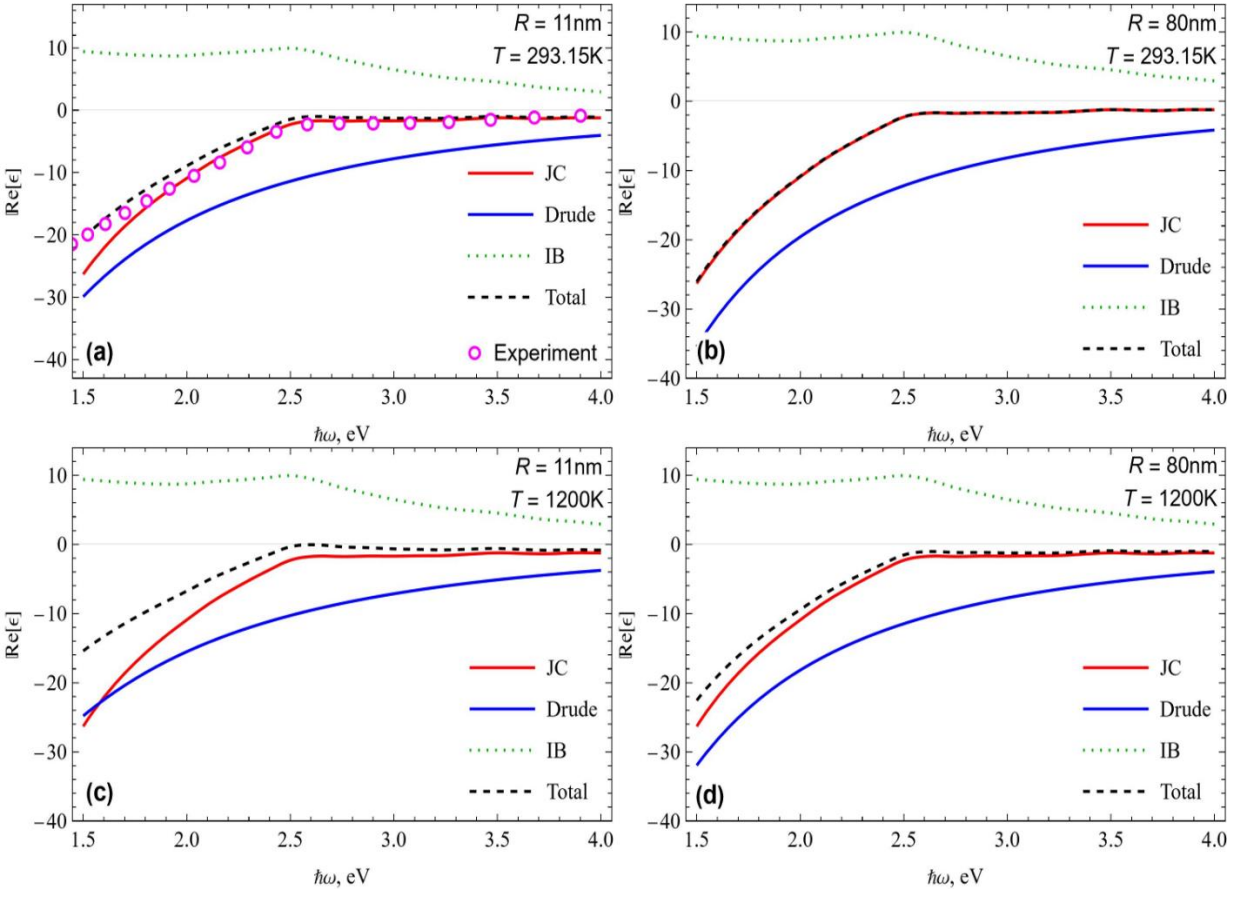

Fig. 4. Real parts of dielectric permittivity for NP with linear size of 11 nm (a, c) and 80 nm (b, d) at T_0 (a, b) and 1200 K (c, d), respectively.

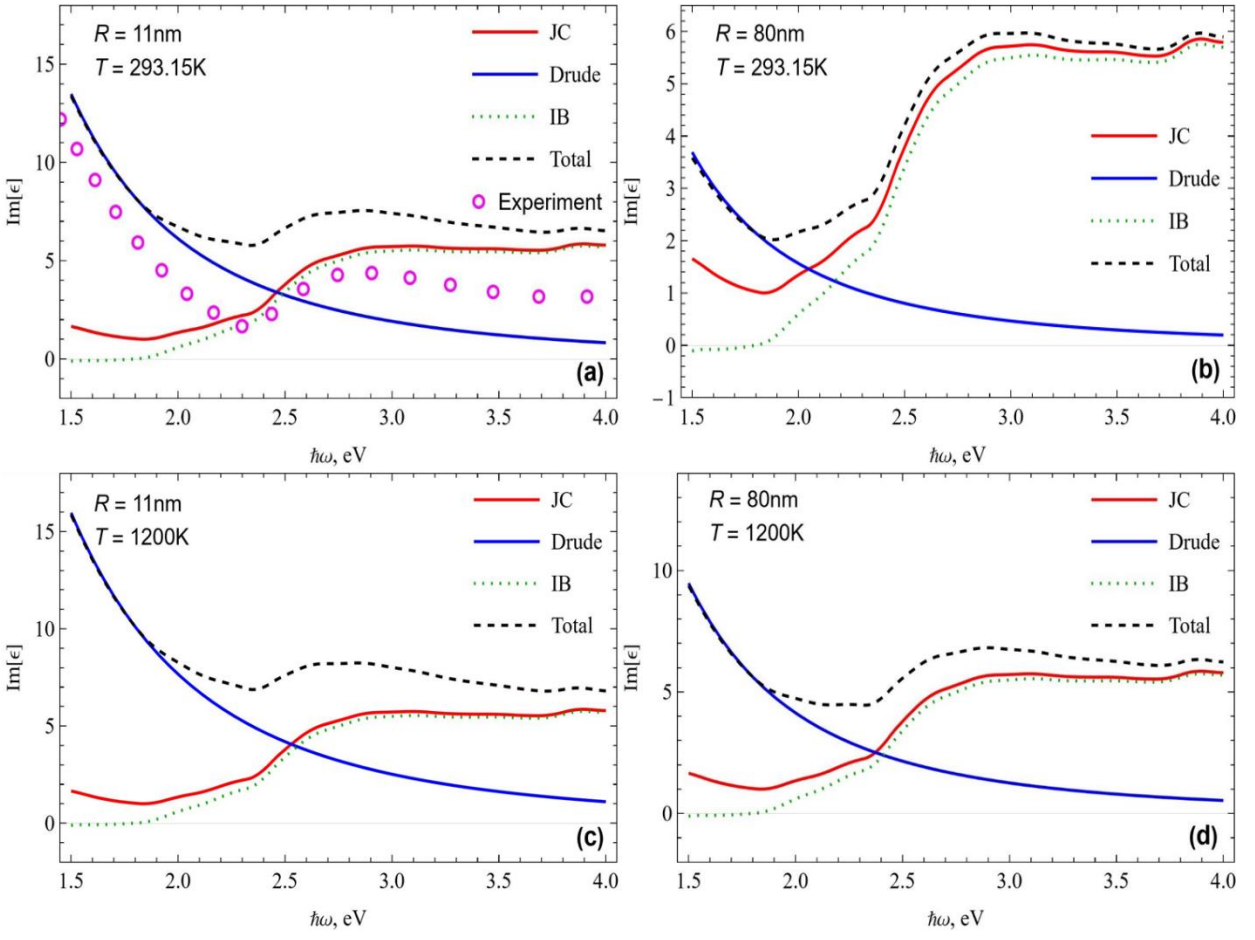

Fig. 5. Imaginary parts of dielectric permittivity for NP with linear size of 11 nm (a, c) and 80 nm (b, d) at T_0 (a, b) and 1200 K (c, d), respectively.

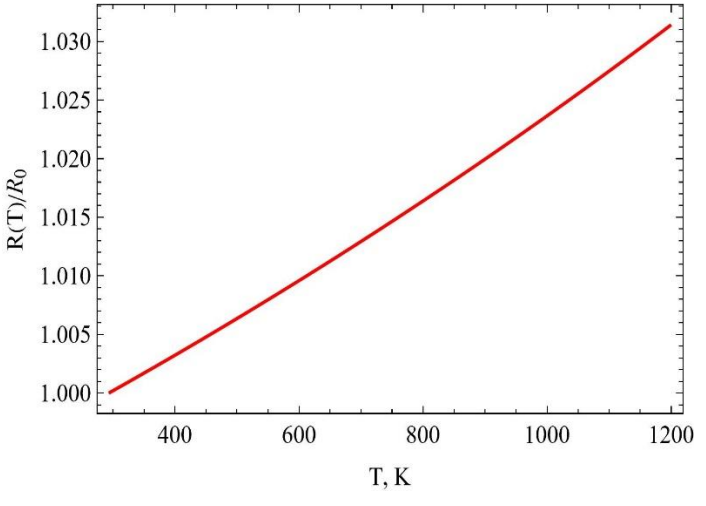

Fig. 6. Thermal expansion of a gold NP from room temperature to 1200 K.

Figure 8 (a) depicts the absorption cross-section for a 20nm nanosphere in silica glass at wide range of temperatures starting from room temperature up to 1200K. It can be seen that with increase in temperature LSPR frequency red-shifts, which is mainly due to the NP's volume expansion.

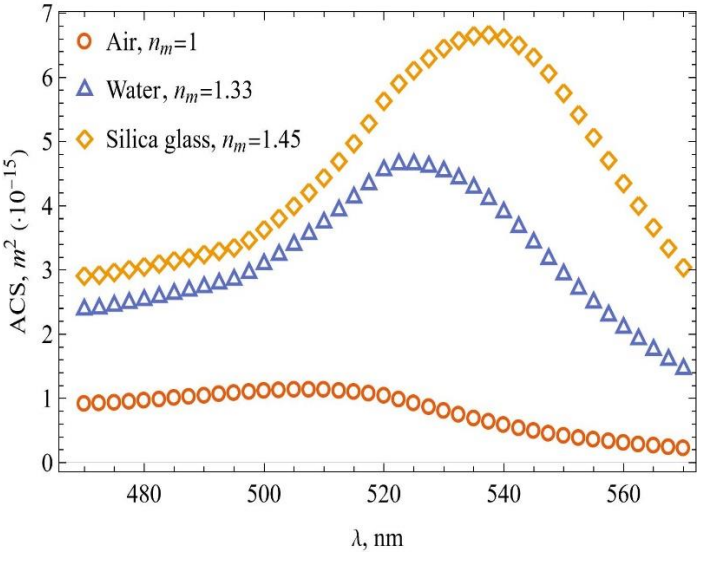

Fig. 7. Absorption cross-section for nanosphere with diameter D = 40 nm in air, water or silica glass host.

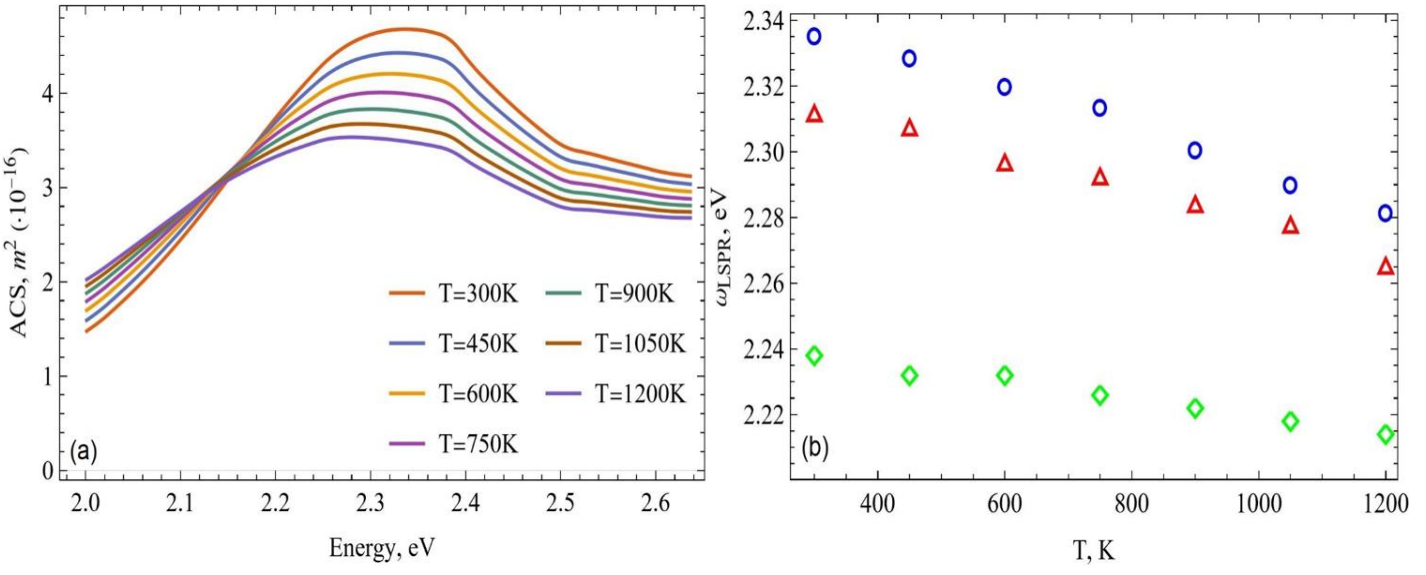

Fig. 8. (a) Absorption cross-section for nanosphere with diameter D = 20 nm in silica glass at different temperatures. (b) LSPR frequency over temperature for different diameters of spherical NPs: 20 nm (circle), 40 nm (triangle), 80 nm (rhombus).

The latter is more clearly depicted in Figure 8(b), which represents the simulated LSPR frequencies for different diameters of nanospheres at different temperatures. The same temperature range as in previous subfigure was considered. The LSPR frequency red-shifts with an increase in NP size or with an increase in temperature. One can also see that the corresponding absorption curves broaden, which can be explained by the increase of the scattering and damping effects [23].

The size dependence of the LSPR curves is primarily shown in Figure 9, which represents the absorption efficiency for nanospheres with 20nm, 40nm and 80nm diameters. It can be seen that there is a broadening of the absorption curves and a red-shift of the plasmon resonance wavelength from 520 nm to 543nm, as it was shown by Jain *et al.* in Ref. [19] and has been observed in the measured optical spectra [38, 48, 49]. The inset represents electric field norm distribution over the central xz plane of the nanosphere with 40nm radius at close to resonance wavelength of 540nm.

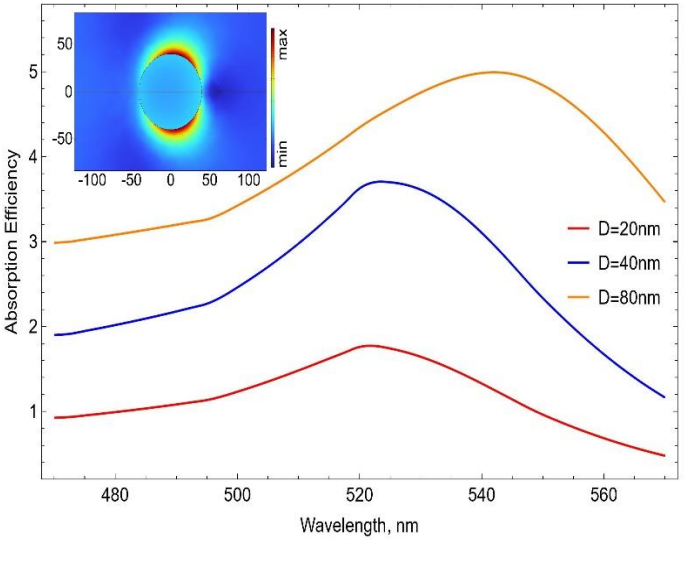

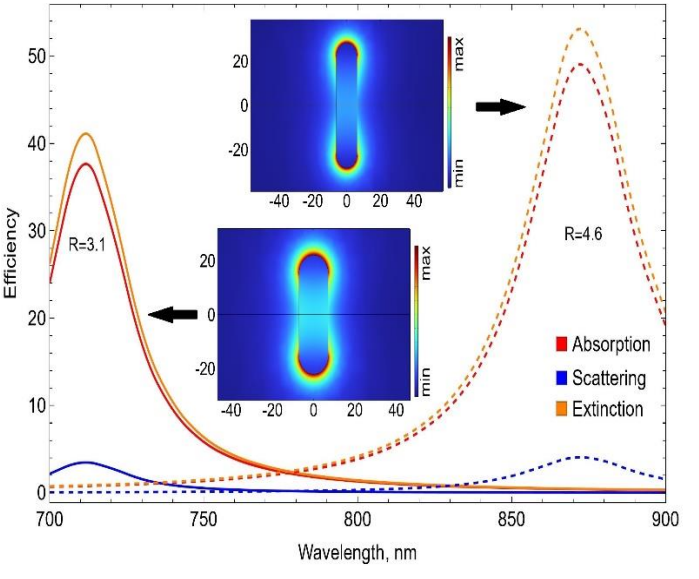

Fig. 9. Absorption efficiencies for nanosphere (D=20, 40, 80 nm) in water. Inset: electric field norm for the nanosphere of 80 nm diameter at 540 nm wavelength.

Fig. 10. Absorption, scattering and extinction efficiencies for gold nanorods with different sizes (R=3.1 and R = 4.6, when r_{eff}=11.43 nm) in water. Inset: electric field norm for the same nanorods at 710 nm and 875 nm wavelengths, respectively.

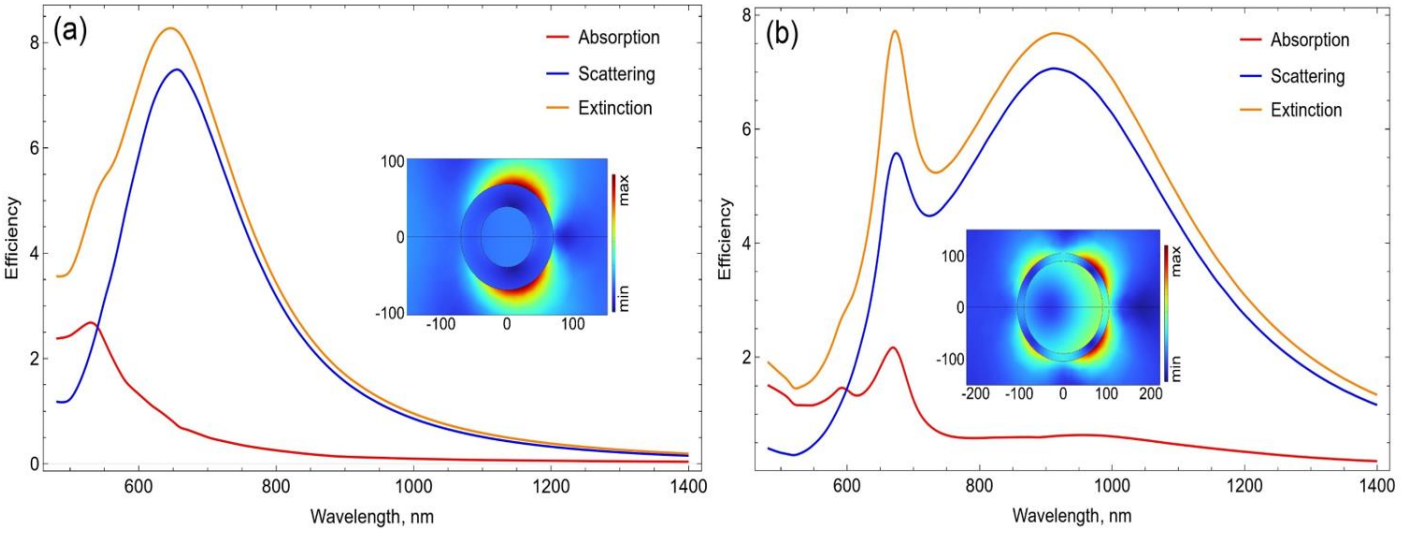

Fig. 11. Absorption, scattering and extinction efficiencies for silica/gold nanoshell with (a) $R_1 = 70$ nm, $R_2 = 40$ nm, (b) $R_1 = 105$ nm, $R_2 = 90$ nm in water. Inset: electric field norm for the same nanoshells at 625 nm and 680 nm wavelengths, respectively.

Let us recall that incident electromagnetic wave travels along the x axis and is polarized along the z axis. The penetration depth, calculated with $l^{-1} = (2\pi/\lambda)\mathrm{Im}[n(\lambda)]$ [44], where $n(\lambda)$ is the refractive index at wavelength λ, gives values of l around 30nm in the considered range of wavelengths.

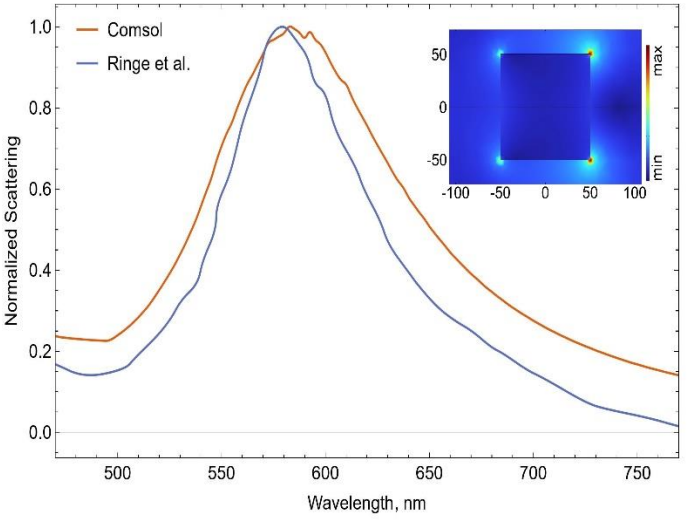

Fig. 12. Normalized scattering of gold nanocube (d = 100 nm) in air. Inset: electric field norm for the nanocube at 575 nm wavelength.

In Figure 10, the absorption, scattering and extinction efficiencies for a nanorod placed in the water are presented. Similar to Jain *et al.*, the gold nanorod was constructed here with the help of a cylinder capped with two hemispheres. Two parameters are used to characterize the nanorod: effective radius, given by $r_{eff} = (3V/4\pi)^{1/3}$, where V is the volume of the nanorod, and aspect ratio R, which is the ratio of the nanorod dimension along the long axis to the one along the short axis. In the current discussion, a nanorod with effective radius $r_{eff} = 11.43$ nm and aspect ratios R = 3.1 and R = 4.6 is considered. The incident electromagnetic field is polarized along the long axis of the nanorod. It can be seen, that compared to the case of nanospheres the plasmon resonance peak here moves closer to the near-infrared region, which, with further tuning of the effective radius and aspect ratio, can make nanorods extremely useful for biomedical applications, particularly.

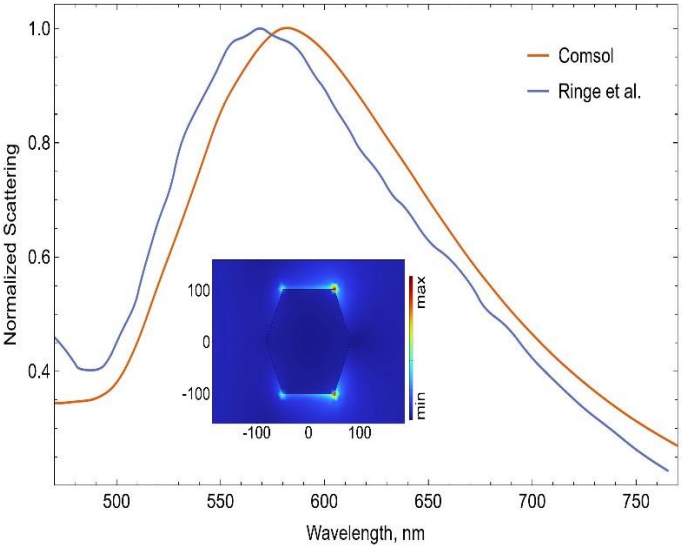

Fig. 13. Normalized scattering of icosahedron-shaped gold NP (d = 100 nm) in air. Inset: electric field norm for the icosahedron at 580 nm wavelength.

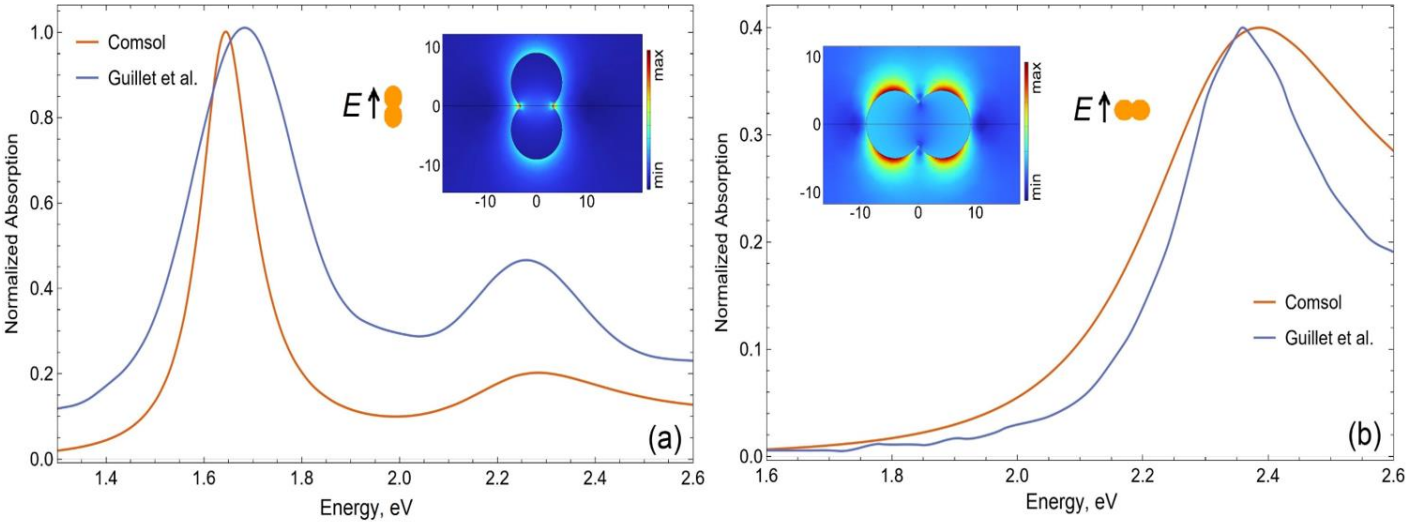

Fig. 14. Normalized absorption of gold nanopeanut (r = 5nm, r_{in} = 3nm) in silica. Inset: electric field norm for the same orientations of nanopeanuts at 750 nm (1.65 eV) and 520 nm (2.38 eV), respectively.

Figure 11 presents the absorption, scattering and extinction efficiencies for silica/gold nanoshell in the water. Nanoshell is described by two radii: total radius R_1 and shell radius R_2. Yet again, it can be seen that the plasmon resonance peak is highly sensitive to core/shell dimensions: it has moved to the near-infrared region and can be tuned by changing the core/shell dimensions. Those results are also in agreement with the ones obtained by Jain *et al.* in Ref. [19], while the latter are not brought here in order to avoid overload on the Figure.

In Figure 12 and 13, our modeled results for the normalized scattering of Au cube and icosahedron both with d=100 nm side length placed in air are being compared with the experimental data from Ref. [50]. The close values obtained for the LSPR wavelengths of these two geometries confirm the findings of Ringe *et al.* that the plasmon length can act as a very important property for describing the size effects of Au NPs, regardless of their shape. Recall that plasmon length is a size parameter, which can be defined for dipolar plasmons equal to the distance between regions of opposite charges created by the electron oscillations.

Figure 14 illustrates the normalized absorption spectrum of gold nanopeanuts with an outer radius (r) of 5 nm and an inner radius (rin) of 3 nm embedded in a silica matrix. The plot shows how the absorption characteristics of these gold nanopeanuts vary across different wavelengths. As the shape and size of these nanoparticles are asymmetrical (peanut-like), the absorption behavior is significantly influenced by the aspect ratio and the orientation of the nanopeanut in relation to the incident light. The inset of the figure provides a visualization of the electric field distribution around the nanopeanuts at two different wavelengths: 750 nm (corresponding to an energy of 1.65 eV) and 520 nm (corresponding to an energy of 2.38 eV). These specific wavelengths are chosen because they correspond to key plasmonic resonances, with 750 nm representing the longer wavelength resonance and 520 nm representing the shorter one [51]. This behavior underpins the potential use of gold nanopeanuts in applications requiring precise control of light-matter interactions, such as in plasmonic sensors or nanophotonic devices.

5. CONCLUSION

In this study, we have developed a comprehensive theoretical model to investigate the localized surface plasmon resonance (LSPR) in gold nanoparticles (Au NPs), accounting for both size and temperature effects. Using the COMSOL Multiphysics simulation software, we modeled a variety of nanoparticle geometries, including nanospheres, nanorods, core/shell structures, nanocubes, icosahedral, and nanopeanut shapes, in different environments (air, water, and silica glass) across a broad temperature range. The dielectric function was formulated as a function of both nanoparticle size and temperature, which allowed for an accurate simulation of the optical properties of Au NPs. The results demonstrate a clear red-shift in the LSPR frequency as both nanoparticle size and temperature increase. This shift is crucial for applications where precise control of optical resonance is required. Additionally, the absorption, scattering, and extinction cross-sections were calculated for the different nanoparticle geometries, confirming that each shape exhibits distinct optical behaviors. These variations in optical properties provide valuable insight into the tunability of Au NPs, which is highly relevant for their application in fields like photothermal therapy, sensing, and medical imaging. Furthermore, the simulation results were compared with

existing literature, showing good agreement and validating the accuracy of our approach. By manipulating nanoparticle size, shape, and environmental conditions, we can achieve targeted control over the optical properties of Au NPs. This tunability is especially beneficial for designing nanoparticles for specific biomedical applications, where factors like biocompatibility and precise light-matter interactions are critical. In conclusion, this work provides a robust theoretical and computational framework for understanding and optimizing the optical properties of Au NPs, paving the way for their further development in various scientific and technological applications. The insights gained from this study can guide the design of gold-based nanomaterials with tailored plasmonic characteristics for use in areas such as diagnostics, drug delivery, catalysis, and environmental sensing. Future studies could explore additional factors such as the effects of different solvents, surrounding materials, and more complex nanoparticle architectures to further refine this model and broaden its applicability.

CONFLICT OF INTEREST

The authors declare that there is no conflict of interests.

ACKNOWLEDGMENT

This work was encouraged by "PhD Support Program" 2022 implemented by the Enterprise Incubator Foundation with the support of PMI Science. M.Ya.V. thanks the Ministry of Science and Higher Education of the Russian Federation (State Assignment 075-03-2024-004/5).

REFERENCES

[1] Colomban, P., **2009**. The use of metal nanoparticles to produce yellow, red and iridescent colour, from bronze-age to present times in lustre pottery and glass: solid state chemistry, spectroscopy and nanostructure. *Journal of Nano Research*, 8, pp. 109-132.

[2] Freestone, I., Meeks, N., Sax, M. and Higgitt, C., **2007**. The Lycurgus cup—a roman nanotechnology. *Gold Bulletin*, *40*, pp.270-277.

[3] Ruivo, A., Gomes, C., Lima, A., Botelho, M.L., Melo, R., Belchior, A. and de Matos, A.P., **2008**. Gold nanoparticles in ancient and contemporary ruby glass. *Journal of Cultural Heritage*, *9*, pp.e134-e137.

[4] Spadavecchia, J., Apchain, E., Albéric, M., Fontan, E. and Reiche, I., **2014**. One-Step Synthesis of Collagen Hybrid Gold Nanoparticles and Formation on Egyptian-like Gold-Plated Archaeological Ivory. *Angewandte Chemie*, *126*(32), pp.8503-8506.

[5] Daniel, M.C. and Astruc, D., **2004**. Gold nanoparticles: assembly, supramolecular chemistry, quantum-size-related properties, and applications toward biology, catalysis, and nanotechnology. *Chemical Reviews*, *104*(1), pp.293-346.

[6] Lal, S., Clare, S.E. and Halas, N.J., **2008**. Nanoshell-enabled photothermal cancer therapy: impending clinical impact. *Accounts of Chemical Research*, *41*(12), pp.1842-1851.

[7] Abadeer, N.S. and Murphy, C.J., **2016**. Recent progress in cancer thermal therapy using gold nanoparticles. *The journal of physical chemistry C*, *120*(9), pp.4691-4716.

[8] Dreaden, E.C., Mackey, M.A., Huang, X., Kang, B. and El-Sayed, M.A., **2011**. Beating cancer in multiple ways using nanogold. *Chemical Society Reviews*, *40*(7), pp.3391-3404.

[9] Kennedy, L.C., Bickford, L.R., Lewinski, N.A., Coughlin, A.J., Hu, Y., Day, E.S., West, J.L. and Drezek, R.A., **2011**. A new era for cancer treatment: gold-nanoparticle-mediated thermal therapies. *Small*, *7*(2), pp.169-183.

[10] Rosi, N.L. and Mirkin, C.A., **2005**. Nanostructures in biodiagnostics. *Chemical Reviews*, *105*(4), pp.1547-1562.

[11] Hainfeld, J.F., Slatkin, D.N., Focella, T.M. and Smilowitz, H.M., **2006**. Gold nanoparticles: a new X-ray contrast agent. *The British Journal of Radiology*, *79*(939), pp.248-253.

[12] Cole, L.E., Ross, R.D., Tilley, J.M., Vargo-Gogola, T. and Roeder, R.K., **2015**. Gold nanoparticles as contrast agents in x-ray imaging and computed tomography. *Nanomedicine*, *10*(2), pp.321-341.

[13] Ghosh, P., Han, G., De, M., Kim, C.K. and Rotello, V.M., **2008**. Gold nanoparticles in delivery applications. *Advanced Drug Delivery Reviews*, *60*(11), pp.1307-1315.

[14] Pissuwan, D., Niidome, T. and Cortie, M.B., **2011**. The forthcoming applications of gold nanoparticles in drug and gene delivery systems. *Journal of Controlled release*, *149*(1), pp.65-71.

[15] Han, G., Ghosh, P. and Rotello, V.M., **2007**. Functionalized gold nanoparticles for drug delivery. *Nanomedicine*, *2*, pp.113-123.

[16] Daraee, H., Eatemadi, A., Abbasi, E., Fekri Aval, S., Kouhi, M. and Akbarzadeh, A., **2016**. Application of gold nanoparticles in biomedical and drug delivery.

Artificial cells, Nanomedicine, and Biotechnology, *44*(1), pp.410-422.

[17] Khan, A.K., Rashid, R., Murtaza, G. and Zahra, A.J.T.R., **2014**. Gold nanoparticles: synthesis and applications in drug delivery. *Tropical Journal of Pharmaceutical Research*, *13*(7), pp.1169-1177.

[18] Dreaden, E.C., Alkilany, A.M., Huang, X., Murphy, C.J. and El-Sayed, M.A., **2012**. The golden age: gold nanoparticles for biomedicine. *Chemical Society Reviews*, *41*(7), pp.2740-2779.

[19] Jain, P.K., Lee, K.S., El-Sayed, I.H. and El-Sayed, M.A., **2006**. Calculated absorption and scattering properties of gold nanoparticles of different size, shape, and composition: applications in biological imaging and biomedicine. *The Journal of Physical Chemistry B*, *110*(14), pp.7238-7248.

[20] Homberger, M. and Simon, U., **2010**. On the application potential of gold nanoparticles in nanoelectronics and biomedicine. *Philosophical Transactions of the Royal Society A: Mathematical, Physical and Engineering Sciences*, *368*(1915), pp.1405-1453.

[21] Kelly, K.L., Coronado, E., Zhao, L.L. and Schatz, G.C., **2003**. The optical properties of metal nanoparticles: the influence of size, shape, and dielectric environment. *The Journal of Physical Chemistry B*, *107*(3), pp.668-677.

[22] Karimi, S., Moshaii, A., Abbasian, S. and Nikkhah, M., **2019**. Surface plasmon resonance in small gold nanoparticles: introducing a size-dependent plasma frequency for nanoparticles in quantum regime. *Plasmonics*, *14*, pp.851-860.

[23] Yeshchenko, O.A., Bondarchuk, I.S., Gurin, V.S., Dmitruk, I.M. and Kotko, A.V., **2013**. Temperature dependence of the surface plasmon resonance in gold nanoparticles. *Surface Science*, *608*, pp.275-281.

[24] Daneshfar, N., **2014**. Temperature dependence of the optical characteristics and surface plasmon resonance of core-shell nanoparticles. *Physics of Plasmas*, *21*(6), p.063301.

[25] Maurya, M.R. and Toutam, V., **2016**. Size-independent parameter for temperature-dependent surface plasmon resonance in metal nanoparticles. *The Journal of Physical Chemistry C*, *120*(34), pp.19316-19321.

[26] Amendola, V., Pilot, R., Frasconi, M., Maragò, O.M. and Iatì, M.A., **2017**. Surface plasmon resonance in gold nanoparticles: a review. *Journal of Physics: Condensed Matter*, *29*(20), p.203002.

[27] Reddy, H., Guler, U., Kildishev, A.V., Boltasseva, A. and Shalaev, V.M., **2016**. Temperature-dependent optical properties of gold thin films. *Optical Materials Express*, *6*(9), pp.2776-2802.

[28] COMSOL Multiphysics® v. 6.1. www.comsol.com. COMSOL AB, Stockholm, Sweden.

[29] Li-Jun, Z., Jian-Gang, G. and Ya-Pu, Z., **2009**. Size-and temperature-dependent thermal expansion coefficient of a nanofilm. *Chinese Physics Letters*, *26*(6), p.066201.

[30] Kreibig, U. and Vollmer, M., **2013**. Optical properties of metal clusters (Vol. *25*). *Springer Science & Business Media*.

[31] Njoki, P.N., Lim, I.I.S., Mott, D., Park, H.Y., Khan, B., Mishra, S., Sujakumar, R., Luo, J. and Zhong, C.J., **2007**. Size correlation of optical and spectroscopic properties for gold nanoparticles. *The Journal of Physical Chemistry C*, *111*(40), pp.14664-14669.

[32] Drude, P., **1900**. Zur elektronentheorie der metalle. *Annalen der Physik*, *306*(3), pp.566-613.

[33] Drude, P., **1900**. Zur elektronentheorie der metalle; II. Teil. galvanomagnetische und thermomagnetische effecte. *Annalen der Physik*, *308*(11), pp.369-402.

[34] Alvarez, M.M., Khoury, J.T., Schaaff, T.G., Shafigullin, M.N., Vezmar, I. and Whetten, R.L., **1997**. Optical absorption spectra of nanocrystal gold molecules. *The Journal of Physical Chemistry B*, *101*(19), pp.3706-3712.

[35] Sharma, A.K., Pattanaik, H.S. and Mohr, G.J., **2009**. On the temperature sensing capability of a fibre optic SPR mechanism based on bimetallic alloy nanoparticles. *Journal of Physics D: Applied Physics*, *42*(4), p.045104.

[36] Alabastri, A., Tuccio, S., Giugni, A., Toma, A., Liberale, C., Das, G., De Angelis, F., Di Fabrizio, E. and Zaccaria, R.P., **2013**. Molding of plasmonic resonances in metallic nanostructures: Dependence of the non-linear electric permittivity on system size and temperature. *Materials*, *6*(11), pp.4879-4910.

[37] Mortensen, N.A., Raza, S., Wubs, M., Søndergaard, T. and Bozhevolnyi, S.I., **2014**. A generalized non-local optical response theory for plasmonic nanostructures. *Nature Communications*, *5*(1), p.3809.

[38] Link, S. and El-Sayed, M.A., **1999**. Size and temperature dependence of the plasmon absorption of colloidal gold nanoparticles. *The Journal of Physical Chemistry B*, *103*(21), pp.4212-4217.

[39] Etchegoin, P.G., Le Ru, E.C. and Meyer, M., **2006**. An analytic model for the optical properties of gold. *The Journal of Chemical Physics*, *125*(16), p.164705.

[40] Christensen, N.E. and Seraphin, B.O., **1971**. Relativistic band calculation and the optical properties of gold. *Physical Review B*, *4*(10), p.3321.

[41] Johnson, P.B. and Christy, R.W., **1972**. Optical constants of the noble metals. *Physical review B*, *6*(12), p.4370.

[42] Yushanov, S., Crompton, J.S. and Koppenhoefer, K.C., **2013**, October. Mie scattering of electromagnetic waves. In *Proceedings of the COMSOL Conference* (Vol. *116*).

[43] RF Module User's Guide. (n.d.). [online] Available at: https://doc.comsol.com/6.0/doc/com.comsol.help.rf/RFModuleUsersGuide.pdf [Accessed 13 Jan. 2023].

[44] Gonçalves, M., Melikyan, A., Minassian, H., Makaryan, T., Petrosyan, P. and Sargsian, T., **2021**, February. Interband, Surface Plasmon and Fano Resonances in Titanium Carbide (MXene) Nanoparticles in the Visible to Infrared Range. *Photonics*, *8*(2), p.36.

[45] Rakić, A.D., Djurišić, A.B., Elazar, J.M. and Majewski, M.L., **1998**. Optical properties of metallic films for vertical-cavity optoelectronic devices. *Applied optics*, *37*(22), pp.5271-5283.

[46] Olmon, R.L., Slovick, B., Johnson, T.W., Shelton, D., Oh, S.H., Boreman, G.D. and Raschke, M.B., **2012**. Optical dielectric function of gold. *Physical Review B*, *86*(23), p.235147.

[47] Babar, S. and Weaver, J.H., **2015**. Optical constants of Cu, Ag, and Au revisited. *Applied Optics*, *54*(3), pp.477-481.

[48] Rosenblatt, G., Simkhovich, B., Bartal, G. and Orenstein, M., **2020**. Nonmodal plasmonics: Controlling the forced optical response of nanostructures. *Physical Review X*, *10*(1), p.011071.

[49] Bohren, C.F. and Huffman, D.R., **2008**. Absorption and scattering of light by small particles. *John Wiley & Sons.*

[50] Ringe, E., Langille, M.R., Sohn, K., Zhang, J., Huang, J., Mirkin, C.A., Van Duyne, R.P. and Marks, L.D., **2012**. Plasmon length: a universal parameter to describe size effects in gold nanoparticles. *The journal of Physical Chemistry Letters*, *3*(11), pp.1479-1483.

[51] Guillet, Y., Charron, E. and Palpant, B., **2009**. Spectral dependence of the ultrafast optical response of nonspherical gold nanoparticles. *Physical Review B*, *79*(19), p.195432.

